Hindawi
International Journal of Chemical Engineering
Volume 2024, Article ID 2804165, 8 pages
https://doi.org/10.1155/2024/2804165

Research Article

Optimum Green Synthesis, Characterization, and Antibacterial Activity of Silver Nanoparticles Prepared from an Extract of *Aloe fleurentinorum*

Yasmin M. S. Jamil,[1] **Ahmed N. Al-Hakimi**,[2,3] **Hussein M. A. Al-Maydama**,[1] **Ghadeer Y. Almahwiti**,[1] **Ashwaq Qasem**,[4] **and Sayed M. Saleh**[2,5]

[1]*Department of Chemistry, Faculty of Science, Sana'a University, Sana'a, Yemen*
[2]*Department of Chemistry, College of Science, Qassim University, Buraidah 51452, Saudi Arabia*
[3]*Department of Chemistry, Faculty of Science, Ibb University, Ibb, Yemen*
[4]*Qingdao Institute of Bioenergy and Bioprocess Technology, Chinese Academy of Science, Qingdao 266101, China*
[5]*Department of Petroleum Refining and Petrochemical Engineering Department, Faculty of Petroleum and Mining Engineering, Suez 43721, Egypt*

Correspondence should be addressed to Yasmin M. S. Jamil; y.jamil@su.edu.ye

Received 21 December 2023; Revised 29 January 2024; Accepted 6 February 2024; Published 26 February 2024

Academic Editor: Kedhareswara Sairam Pasupuleti

The synthesis of metal nanoparticles through the use of plant extract is a process that is not only simple but also inexpensive, quick, and favorable to the environment. As a result, it is utilized in a wide variety of fields. When synthesizing silver nanoparticles (AgNPs), several different kinds of plant extracts were utilized. The manufacture of silver nanoparticles was carried out in this study using an environmentally friendly technique. The aqueous extract of the Aloe fleurentinorum plant was utilized as a stabilizing and reducing agent. To determine the optimal conditions for the synthesis of silver nanoparticles, it was necessary to investigate the impact of several parameters on the process. These parameters included the reactant volume ratio, pH values, temperature, and reaction time. To get crystallite and stable silver nanoparticles, an aqueous solution of $AgNO_3$ (0.01M) was added to an aqueous extract of Aloe fleurentinorum plant at a temperature of 60 degrees Celsius and a pH of 8. The mixture was then stirred with a magnetic stirrer for ninety minutes (90 minutes). Using a variety of methods (UV-vis spectrophotometer, FTIR, XRD, SEM, EDX, and XPS), several approaches were utilized to investigate and describe the green-produced AgNPs. Through the use of the SEM method, it was demonstrated that the morphology of AgNPs is tetrahedral. It was determined using X-ray diffraction that the size of crystalline AgNPs was 26.7 nm. AgNPs that have been optimally synthesized have antibacterial properties that are both significant and effective against various bacterial species that have been tested at varying doses.

1. Introduction

Nanotechnology is an intriguing discipline that investigates the development and manipulation of nanomaterials, which are very small particles that range in size from one nanometer to one hundred nanometers [1, 2]. These particles have many promising applications in various sectors, such as health [3], agriculture [4], cosmetics [5], food [6], optics [7, 8], cancer therapy [9], catalysis [10, 11], and more. Metal oxide nanoparticles (MNPs) that are manufactured utilizing environmentally acceptable technologies are gaining interest because they are energy-efficient, safe, cost-effective, and environmentally friendly [12, 13]. Compared to their bulk material, MNPs exhibit notably different features in terms of morphology, surface chemistry, physical characteristics, and optical properties [14, 15].

Nanomaterial researchers have paid particular attention to AgNPs among other MNPs because of their unique characteristics and multifunctionality. Manufacturing fabrication of numerous devices, optical sensors, electrical

conductors, catalysts, and medication administration are some of the most remarkable inherent qualities [15, 16]. In addition, lotions, sunscreen products, and ointments are made using AgNPs [17, 18]. The AgNPs have also shown significant antimicrobial potential [19, 20]. There are three main ways that NPs are often made: chemically, physically, and by green synthesis [21, 22]. Physical nanomaterial production techniques need heating and pressurized environments, as well as costly machinery. Serious environmental and human health risks are associated with using various hazardous solvents, expensive metal salts, stabilizers, and reductants in the chemical synthesis of AgNPs [23, 24]. These limitations restrict the usefulness of physicochemical approaches to nanoparticle manufacturing.

Therefore, a simple, cost-effective, eco-friendly, and fast approach is needed. The environmentally friendly route-assisted manufacture of MNPs has garnered much interest owing to the fact that it is risk-free. Green production may be a good alternative to several physicochemical procedures because of their safety, cheap cost, low toxicity, and repeatability. Additionally, green production makes producing AgNPs on a large scale easier. Many research papers have described the creation of silver nanoparticles (AgNPs) from plants using various plant parts as natural resources. These plant parts include leaves, peels, roots, stems, seeds, and fruit. Plant extracts include many phytochemicals, including polyphenols, proteins, enzymes, amino acids, vitamins, polysaccharides, aldehydes, and ketones. These phytochemicals can decrease metal ions and stable nanoparticles to the appropriate shapes and sizes. The number of solvent-based research studies that have been published up to this point on the environmentally friendly manufacturing, characterization, and bio-potential of AgNPs is limited [25].

Phytochemical or plant-based synthesis of nanoparticles using different plant extracts as reducing agents and stabilizing agents instead of chemical or high radiation beams [22] because they contain carbohydrates, proteins, fats, and secondary metabolites such as flavonoids, terpenoids, alkaloids, and polyphenols [26]. The extracts could be used from different plant parts, such as leaves, roots, bark, fruits, seeds, stems, flowers, and oil [27]. Yemen is a rich country for medical exceptive plants and herbs. Still, most current research focuses on chemical and pharmaceutical studies, and only some researchers use these plants for nanoparticle synthesis.

Aloe is a monocotyledon plant genus from the Liliaceae family [28, 29]. *Aloe* L. genus includes more than 600 subspecies and varieties [30]. It is widespread in Asia but only in Southwest Arabia, Socotra, and India [29]. *Aloes* have boat-shaped and succulent leaves [31]. From the previous research, *Aloes* have cytotoxic properties, so it was used as an antibacterial [32]. The *Aloe* L. genus in Yemen is presented by 20 species, including *Aloe fleurentinorum* Lavranos and Newton [29, 33]. *Aloe fleurentinorum* is characterized by stemless armed leaves, rosulate, and lanceolate at the apex surface, which is dark green, very thick, fresh, rough, and without teeth (Figure 1). *Aloe fleurentinorum* occurs on the eastern rain-shadowed slopes of Yemen mountains and Asir region "Saudi Arabia" [29]. Previous studies about *Aloe fleurentinorum* focused on phytochemical screening (Scheme 1) and antimicrobial activities. Moreover, many researchers have used the green method of *Aloe vera* species to synthesize nanoparticles. This work aims to study the physical and biological characteristics of AgNPs synthesized by an ecofriendly route using an aqueous extract of the *Aloe fleurentinorum* plant grown in Yemen.

2. Materials and Methods

2.1. Materials. The *Aloe fleurentinorum* plant was collected from Sana'a in Yemen, silver nitrate (United Kingdom), ammonia solution, absolute ethanol, and deionized water from a science college laboratory.

2.2. Characterization and Measurement Techniques. The synthesis's pH values were adjusted using a METROHM pH meter. The optimal conditions of nanoparticle synthesis were observed and checked by a SPECTROD200 (Analytik Jena) An ultraviolet and visible double-beam spectrophotometer was used with a wavelength range from 300 to 700 nm. The molecules, present as a capping reduction agent for nanoparticles, were characterized using (FTIR) Fourier transform infrared, which was used from a 4000 to 400 cm^{-1} range of wavenumber. The AgNPs structure and crystalline properties were studied using XD-2 (Shimadzu ED-720) powder X-ray diffractometer at a voltage of 36 kV and a current of 20 mA using CuK (α) radiation in the range of $5^{\circ} < 2\theta < 75^{\circ}$ a wavelength of 1.54056 A° at 1° min^{-1} scanning rate. The morphology of the AgNPs was observed by QUANTA FEC 250 SEM. The X-ray Photoelectron Spectroscopy (XPS) analyses were applied using a K-ALPHA (Thermo Fisher Scientific, Waltham, MA, USA) with monochromatic X-ray K-alpha radiation −10 to 1350 eV spot size 400 μm at pressure 10^{-9} mbar with full-spectrum pass energy 200 eV and narrow-spectrum 50 eV.

2.3. Methods

2.3.1. The Aloe fleurentinorum Plant Extract Preparation. The *Aloe fleurentinorum* leaves (AFL) were collected from Dr Hassan Ebrahim Garden, Sana'a, Yemen, during the summertime of 2022. The plant (AFL) underwent multiple washes utilizing distilled water. Then, dried at room temperature for three days away from sunlight, the plant was ground to a fine powder. Then, 5 g of (AFL) powder was immersed in 100 mL deionized water and stirred for 30 min utilizing a magnetic stirrer. At 60°C, the extract was cooled at room temperature and filtered.

2.3.2. Green Synthesis of Silver Nanoparticles (AgNPs). A 0.01 M of silver nitrate (0.17 gm of $AgNO_3$ in 100 mL deionized water) was prepared, and aqueous AFL extract was added to $AgNO_3$ solution with different conditions as the volume ratio of reactant, pH value, and the reaction temperature to get the optimal conditions for synthesis nanoparticles.

Figure 1: *Aloe fleurentinorum* general view [30].

Scheme 1: Qualitative constituents of *Aloe fleurentinorum* aqueous leaf extract.

(1) The Optimum Volume Ratio of Reactants. 4 volume ratio (1 : 1, 1 : 2, 1 : 3, 1 : 4) solutions were prepared by mixing a fixed volume of AFL extract (10 mL) with a certain volume of $AgNO_3$ (0.01 M), (10, 20, 30, 40 mL); they were labeled with G_1, G_2, G_3, and G_4 and the pH value of the reaction adjusted up to 7 by dill. NH_3 solution.

(2) The Optimal pH Value. After selecting the optimal volume ratio, 4 solutions were prepared (G_5, G_6, G_7, G_8) by changing the pH values of the reaction by adding diluted NH_3 solution at pH 5.7, 7, 8, and 9.

(3) The Optimal Reaction Temperature. Using fixed values of volume ratio and pH at the optimal conditions, 5 solutions were prepared at different temperatures (20, 35, 60, 70, 80°C) and labeled as G_9, G_{10}, G_{11}, G_{12}, G_{13}.

(4) The Optimal Reaction Time. One sample was prepared using the optimal conditions by mixing the optimal volume ratio (1 : 1), at the optimal pH value (pH = 8), and the optimal temperature (60°C) with continuous stirring until 2 h.

2.3.3. Antibacterial Activity Studies. To investigate the biological activity of AgNPs produced using *Aloe fleurentinorum* leaf extract, the antibacterial activities of AgNPs were studied against different bacterial types using the agar diffusion technique. The studies were against 2 types of Gram-positive bacteria (*Staphylococcus Aureus* and *Bacillus Subtilis*) and 2 types of Gram-negative bacteria (*Escherichia Coli* and *Salmonella Typhi*). The AgNPs effect on bacteria was tested with a 100% solution as a synthesized AgNPs at the optimal conditions as a stock solution, and three different dilutions from the stock (75%, 50%, 25%), and they were labeled as G_{100}, G_{75}, G_{50}, G_{25}. After inoculating the bacterial cells on Petri dishes, the holes were made in the bacterial dishes and filled with different concentrations of synthesized AgNPs. Then, the dishes were incubated at 37°C for a full one-day duration. The antibacterial activities of AgNPs samples were determined by measuring the inhibition zones around the samples.

3. Results and Discussion

3.1. Ultraviolet-Visible Spectroscopy Characterization

3.1.1. The Volume Ratio of Reactant Effect. The comparison of the UV-vis absorption spectrum of the extract in Figure S1 (at supplementary materials) with the spectra of the green synthesized silver nanoparticles verified the AgNPs formation at a constant volume of AFL (10 ml). It monitored the formation of AgNPs after different volumes of $AgNO_3$ (0.01 M) from 10 ml to 40 ml. The absorbance peaks indicate that increasing $AgNO_3$ volume from 10 ml to 40 ml causes a decrease in AgNPs formation. That means the sample G1, which had the reactants' 1 : 1 volume ratio, had the highest absorption. So, the optimal volume ratio determined for the green synthesized AgNPs is G1.

3.1.2. The pH Value Effect. Studying the effect of pH on the formation of Ag-NPs by changing the pH values from 5.7 to 9 is shown in Figure S2 (at supplementary materials). The UV-vis absorbance peak decreased, then increased, then decreased, and the absorbance peaks shifted to a blue wavelength (425 nm). This indicates the decrease of AgNP diameter. So, the optimal pH value for the green synthesized AgNPs is G7 at pH = 8.

3.1.3. The Temperature of the Reaction. The silver nanoparticles' UV-visible spectra synthesized at various temperatures are shown in Figure S3 (at supplementary materials). It shows that the absorbance peak increases and then decreases. The maximum absorbance of sample G11 is at temperature 60°C. That indicates the optimal reaction temperature at this value.

3.1.4. The Reaction Time. As shown in Figure S4 (at supplementary materials), the absorbance range gradually increased as the reaction time increased and the color intensity increased with the incubation duration. This indicates an increase in the formation of AgNPs with increasing color intensity with time.

3.1.5. Band Gap Energy Determination. The semiconductor gap refers to the spatial separation between the valence and conductance bands, which are devoid of electrons. The

semiconductor's absorption threshold determines the minimum amount of photon energy required to generate photoelectrons and holes. By using the absorption spectra of the optimal conditions, the band gap in Figure S5 (at supplementary materials) was determined for synthesized AgNPs using Tauc's equation $((\alpha h\upsilon)^2 = k(h\upsilon - E_g))$, as shown in Figure S5 (at supplementary materials).

3.2. Fourier Transform Infrared Characterization. The method used to show the structure and function groups presented in materials is the Fourier transform infrared spectra. FTIR was shown in Figure S6 (at supplementary materials) for *Aloe fleurentinorum* leaf extract and the synthesized AgNPs. It shows a broad stretching vibration band of OH for AFL extract at 3250 cm^{-1}, which decays in intensity of AgNPs IR spectra. That indicates this bond is used in the reduction process for silver ions to AgNPs [34]. Likewise, the stretching vibration band of the C=O group at 1520 cm^{-1} and the curvature vibration band of the OH group at 1440 cm^{-1} are utilized in the synthesis of AgNPs as a reducing, capping, and stabilizing agent.

3.3. X-Ray Diffraction Characterization. X-ray diffraction is a significant and effective technique for verifying the elements' identity in the prepared nanoparticle samples. Figure 2 shows the X-ray diffraction patterns of dried Ag nanoparticles synthesized at 60°C using AFL extract and at pH 8. Comparing these positions of peaks with standard XRD cards shows the AgNPs' crystallinity phase. The peaks at 38.51°, 44.79°, and 77.8° correspond to the planes (111), (200), and (311) for Ag (JCPDS no. 87-0719). This revealed that silver nanoparticles have a face-centered shape. The silver nanoparticles formed sizes are estimated to be 26.87 nm, determined using Debye–Scherer's equation (1).

$$D = \frac{K\lambda}{\beta \cos\theta}, \tag{1}$$

where D is the average particle size, K is a constant (0.94), λ is the wavelength of the x-ray (1.5406 A°), β is the full width at half maximum of the peak (rad) (FWHM), and θ is the position of the diffraction peak.

The microstrain is determined utilizing equation (2). The microstrain and crystalline size values are displayed in Table 1.

$$\text{strain} = \frac{\beta}{4\tan\theta}. \tag{2}$$

The $(a = b = c)$ are the lattice parameters for the synthesized AgNPs, which have a face-centered cubic (FCC) crystallinity, were determined using equation (3), and from these values, the volume was calculated by equation (4).

$$a = d\sqrt{h^2 + k^2 + l^2}, \tag{3}$$

$$V = a^3, \tag{4}$$

where (h, k, l) are the Miller indices and d is the plane spacing determined through Bragg's equation (5).

$$d = \frac{\lambda}{2\sin\theta}. \tag{5}$$

The lattice parameters (a, b, and c) (Table 2) are practically indistinguishable from those announced in the (JCPDS no. 87-0719) card for AgNPs.

A dislocation is an imperfection in a crystal related to the lattice existing in various crystal pieces. The dislocation density can be determined utilizing equation (6). The values of dislocation density are displayed in Table 2.

$$\delta = \frac{1}{\widehat{D}2}. \tag{6}$$

From the XRD pattern, the porosity of the synthesized samples was determined. The percentage of porosity was determined and tabulated in Table 2, as indicated by equation (7) [35], where ρ_x is the theoretical density and ρ is the determined density from X-ray data utilizing the equation formula (8).

$$\text{Porosity \%}\ (P) = \left[1 - \frac{\rho}{\rho_x}\right] \times 100, \tag{7}$$

$$\rho = \frac{\text{ZM}}{\text{NV}}. \tag{8}$$

Z is the number of chemical units in one crystal unit cell = 4, M is the molecular weight (107.87 g/mole), N is Avogadro's number, and V is the volume.

3.4. Energy Spectrum Component Analysis. X-ray energy dispersive spectrometry. The elements were analyzed using energy-dispersive X-ray spectrometry (EDX). EDX images of Ag-NPs are displayed in Figure 3, revealing peaks corresponding to elements such as Ag, O, N, C, and others present in the plant. This verifies the utilization of the Aloe fleurentinorum plant as a reducing agent in producing silver nanoparticles. Table 3 exhibits the elemental analysis of the synthesized silver nanoparticles by X-ray energy dispersive spectrometry.

3.5. Scanning Electron Microscopy (SEM). The conducted SEM images of the silver nanoparticles (AgNPs) demonstrated their synthesis as tetrahedral particles, as seen in Figure 4. The plant known as *Aloe fleurentinorum* has significant promise in silver nanoparticle synthesis. Using higher-density scanning electron microscopy (SEM) techniques facilitated the identification of silver nanoparticles exhibiting a tetrahedral shape, as visually depicted in Figure 4. The utilization of *Aloe fleurentinorum* plant extract in synthesizing silver nanoparticles resulted in the successful formation of silver nanostructures, as evidenced by the scanning electron microscopy (SEM) image.

3.6. XPS Analysis. The XPS assessment was carried out to analyze the structure of the silver nanoclusters as well as their chemical makeup (Figure 5). The findings demonstrate two distinct peaks, 367.37 eV (Ag 3d5/2) and 373.52 eV (Ag

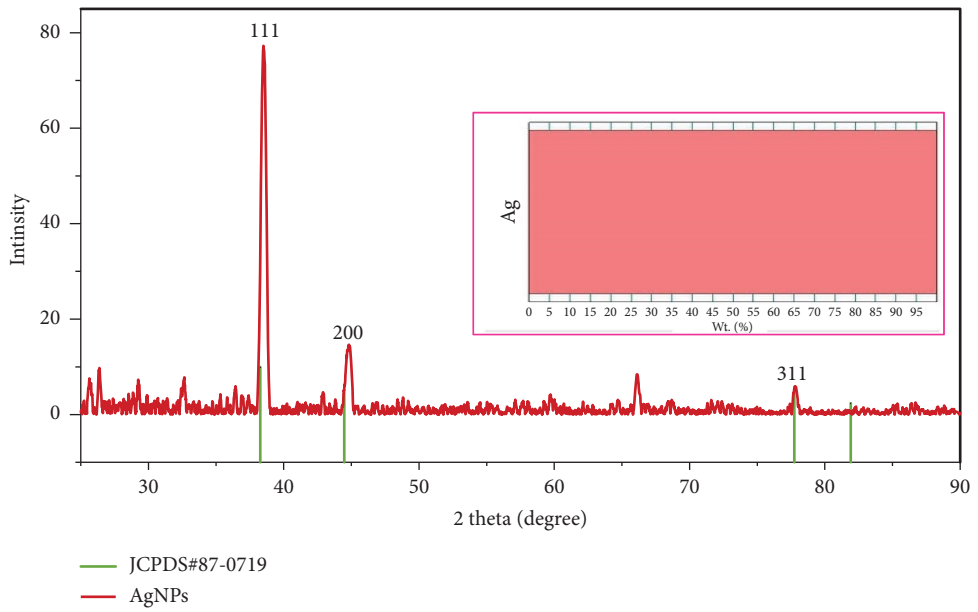

Figure 2: XRD pattern of AgNPs.

Table 1: Calculated interplaner d-spacing, crystalline sizes, and microstrain ofAgNPs.

2θ (°)	d (A°)	FWHM (degree)	D (nm)	Strain $(\varepsilon) \times 10^{-4}$
38.51	2.334	0.4325	20.314	6.593
44.79	2.021	0.44156	20.316	7.939
77.81	1.226	0.26651	39.991	9.385
Average			26.874	7.973

Table 2: Lattice parameters, porosity, X-ray density, and dislocation density of AgNPs.

2θ (°)	h	k	l	d (A°)	a (A°)	V (A°^{3})	δ (nm^{-2})	ρ (g/cm^3)	ρ_x (g/cm^3)	Porosity (%)
38.51	1	1	1	2.334	4.0436	66.116	0.002423	10.837	10.617	2.07301
44.79	2	0	0	2.021	4.0419	66.031	0.002423	10.851		2.20381
77.81	3	1	1	1.226	4.0663	67.24	0.000625	10.656		0.36732
Average				1.86	4.0506	66.776	0.001824	10.730		1.54804

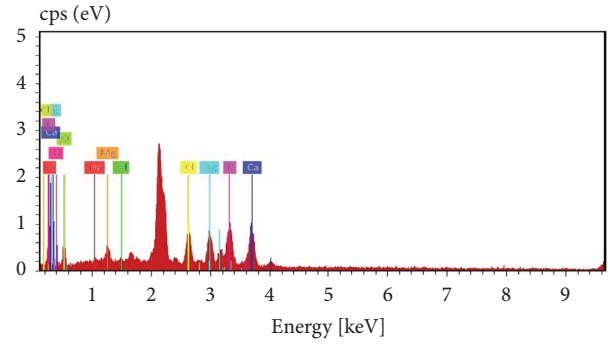

Figure 3: EDX patterns of AgNPs synthesized based on *Aloe fleurentinorum* plant.

3d3/2). In addition, the fact that the binding energy of Ag 3d5/2 is in the middle of the range for Ag (0) and Ag(I), which is between 366.42 and 374.26 eV, indicates that Ag (0) is present [1]. The fact that the peaks moved to inferior binding energies demonstrates that the chemical behavior of the surface Ag atoms changed. This change in chemical nature might be attributed to a combination of Ag (0) and Ag (I), as seen by the shift in the peaks. The structure of tryptophan is similar to that of the skeleton of an amino acid, and its functional groups include carboxyl and amino groups.

3.7. Antibacterial Activity of AgNPs. The antibacterial activity of the green synthesized AgNPs by *Aloe Fleurentinorum* leaves the extract at optimal conditions against two types of Gram-Positive bacteria (*Staphylococcus Aureus* and *Bacillus Subtilis*) and two types of Gram-Negative bacteria (*Escherichia Coli* and *Salmonella Typhi*) effects are shown in Figure S7 (at supplementary materials). The inhibition zones against different bacterial strains were shown for AgNPs' synthesized by AFL extract ranging from

Table 3: Elemental analysis of the as-synthesized AgNPs.

Element	At. No.	Netto	Mass (%)	Mass norm (%)	Atom (%)	Abs. error (%) (1 sigma)	Rel. error (%) (1 sigma)
Oxygen	8	840	5.82	23.31	35.57	1.41	24.23
Calcium	20	3095	4.73	18.95	11.55	0.2	4.13
Silver	47	3156	4.58	18.33	4.15	0.2	4.33
Carbon	6	971	3.51	14.04	28.55	0.83	23.55
Potassium	19	2941	3.09	12.4	7.74	0.14	4.55
Chlorine	17	2182	1.86	7.46	5.14	0.1	5.62
Magnesium	12	561	0.59	2.37	2.38	0.07	12.35
Nitrogen	7	46	0.59	2.35	4.09	0.43	73.41
Sodium	11	119	0.17	0.66	0.71	0.05	28.88
Aluminum	13	34	0.03	0.13	0.12	0.01	20

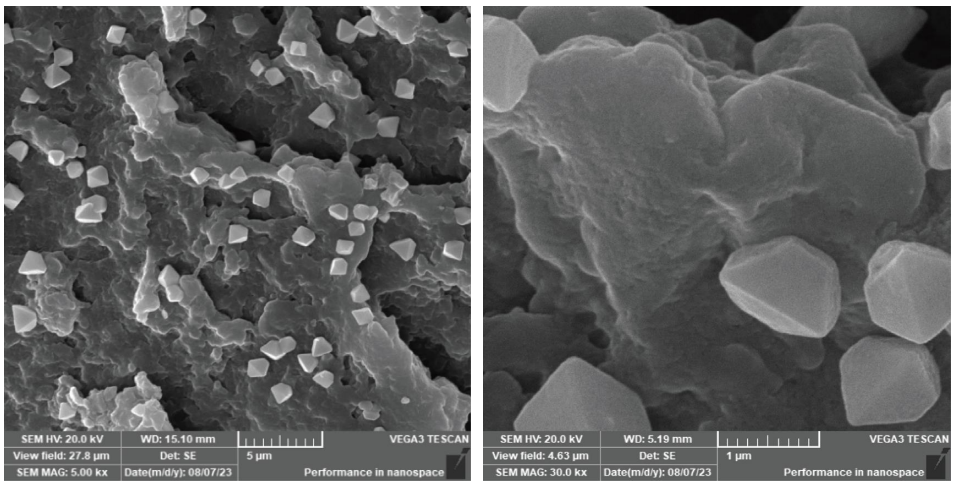

Figure 4: SEM images of AgNPs.

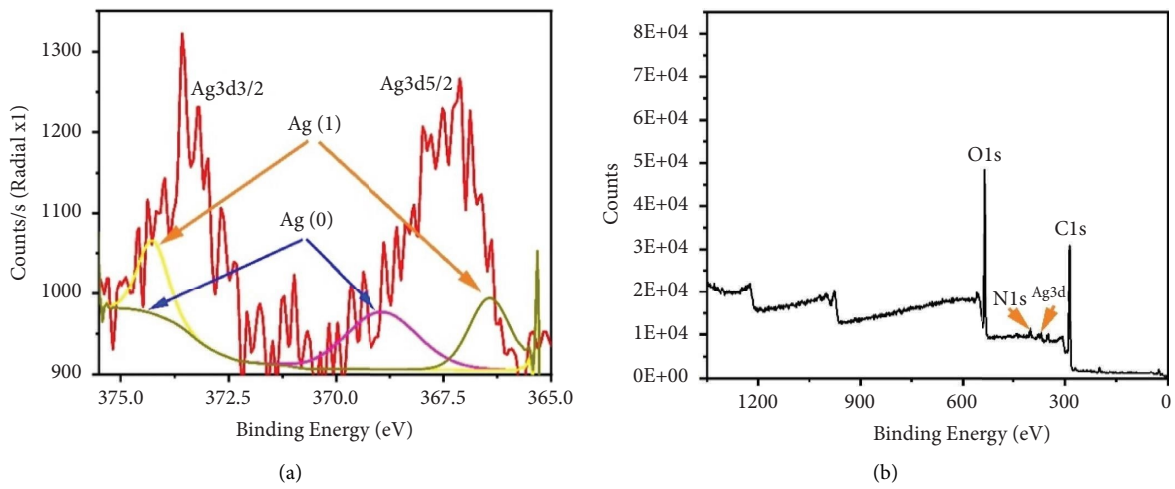

Figure 5: (a) XPS spectra of Ag3d for AgNPs; (b) the whole XPS spectrum of AgNPs.

1 mm to 18 mm. The inhibition zones are listed in Table 4 for the 4 different bacterial strains, which indicate different effects by variation AgNP concentration. The higher inhibition zones were observed on *Escherichia Coli*Gram-negative bacteria, which has a greater inhibition zone for AgNPs at different concentrations (16–18 mm), maybe because of the bacterial cell wall thickness. Gram-positive bacteria have a peptidoglycan thick layer cell wall, which makes them more resistant than Gram-negative species [36, 37]. AgNPs may be synthesized by combining several organic chemicals found in the *Aloe* plant extract with $AgNO_3$. These components include saponin, tannin,

Table 4: The antibacterial activities of the synthesized AgNPs.

Pathogenic bacteria	Bacteria names	Inhibition zones in mm			
		G_{25}	G_{50}	G_{75}	G_{100}
Gram-positive bacteria	*Staphylococcus Aureus*	2	6	9	10
	Bacillus Subtilis	1	1	6	7
Gram-negative bacteria	*Escherichia Coli*	16	16	17	18
	Salmonella Typhi	11	13	14	14

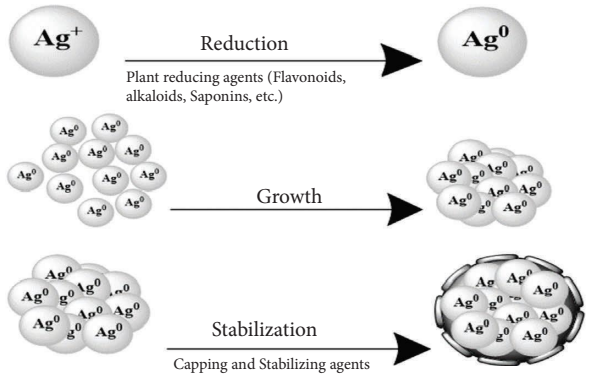

Figure 6: The mechanism of AgNPs formation.

terpenoids, and flavonoids. Green synthesis incorporates these organic molecules shown in Figure 6. As a consequence of the accumulation of these nanocrystals at the cell membrane, the membrane's permeability is increased, ultimately leading to the cell's death [28]. In general, it was observed that the inhibitory activity increased by increasing the concentration of AgNPs.

4. Conclusion

Successfully green synthesized AgNPs using *Aloe fleurentinorum* plant extract were carried out in our research work. UV-vis analysis determined the optimal conditions (V/V ratio, pH, T, and reaction time) for the green synthesized AgNPs. The capping and reducing agents present in the AFL BioSource were identified by FTIR and XPS techniques. The average size of the particles was determined to be 26.8 nm using XRD analysis. SEM images showed the tetrahedral morphology of the synthesized AgNPs. In this work, the antimicrobial activity studies for these synthesized AgNPs revealed a stronger and more promising effect for the Gram-negative bacteria than the Gram-positive bacteria, especially for *Escherichia Coli* species.

Data Availability

All significant data are included in the article.

Conflicts of Interest

The authors declare that they have no conflicts of interest.

Supplementary Materials

Figure S1: the absorbance of AgNPs based on their volume ratio. Figure S2: the absorbance of AgNPs based on pH values. Figure S3: the absorbance of AgNPs at different temperatures. Figure S4: the absorbance of AgNPs based on reaction times. Figure S5: Tauc's plot for the energy band gap of the AgNPs. Figure S6: FTIR of ecofriendly synthesized AgNPs. Figure S7: the test of the synthesized AgNPs antibacterial activities against *Bacillus Subtilis* (a), *Staphylococcus Aureus* (b), *Escherichia Coli* (*c*), *Salmonella Typhi* (d), and the inhibition zones of green synthesized AgNPs in different concentrations (e). (*Supplementary Materials*)

References

[1] S. M. Saleh, M. K. Almotiri, and R. Ali, "Green synthesis of highly luminescent gold nanoclusters and their application in sensing Cu(II) and Hg(II)," *Journal of Photochemistry and Photobiology A: Chemistry*, vol. 426, Article ID 113719, 2022.

[2] R. Ali, B. Alfeneekh, S. Chigurupati, and S. M. Saleh, "Green synthesis of pregabalin-stabilized gold nanoclusters and their applications in sensing and drug release," *Archives of Pharmacy*, vol. 355, no. 4, 2022.

[3] S. P. Thomas, E. M. Al-Mutairi, and S. K. De, "Impact of nanomaterials on health and environment," *Arabian Journal for Science and Engineering*, vol. 38, no. 3, pp. 457–477, 2013.

[4] R. J. Peters, H. Bouwmeester, S. Gottardo et al., "Nanomaterials for products and application in agriculture, feed and food," *Trends in Food Science and Technology*, vol. 54, pp. 155–164, 2016.

[5] G. Fytianos, A. Rahdar, and G. Z. Kyzas, "Nanomaterials in cosmetics: recent updates," *Nanomaterials*, vol. 10, no. 5, p. 979, 2020.

[6] C. F. Chau, S. H. Wu, and G. C. Yen, "The development of regulations for food nanotechnology," *Trends in Food Science and Technology*, vol. 18, no. 5, pp. 269–280, 2007.

[7] S. M. Saleh, F. M. Alminderej, R. Ali, and O. I. Abdallah, "Optical sensor film for metribuzin pesticide detection," *Spectrochimica Acta Part A: Molecular and Biomolecular Spectroscopy*, vol. 229, Article ID 117971, 2020.

[8] S. M. Saleh, R. Ali, M. E. F. Hegazy, F. M. Alminderej, and T. A. Mohamed, "The natural compound chrysosplenol-D is a novel, ultrasensitive optical sensor for detection of Cu(II)," *Journal of Molecular Liquids*, vol. 302, Article ID 112558, 2020.

[9] S. M. Saleh, W. A. El-Sayed, M. A. El-Manawaty, M. Gassoumi, and R. Ali, "An eco-friendly synthetic approach for copper nanoclusters and their potential in lead ions sensing and biological applications," *Biosensors*, vol. 12, no. 4, p. 197, 2022.

[10] S. M. Saleh, "ZnO nanospheres based simple hydrothermal route for photocatalytic degradation of azo dye," *Spectrochimica Acta Part A: Molecular and Biomolecular Spectroscopy*, vol. 211, pp. 141–147, 2019.

[11] M. Tayyab, Y. Liu, Z. Liu et al., "One-pot in-situ hydrothermal synthesis of ternary $In_2S_3/Nb_2O_5/Nb_2C$ Schottky/S-scheme integrated heterojunction for efficient photocatalytic hydrogen production," *Journal of Colloid and Interface Science*, vol. 628, pp. 500–512, 2022.

[12] A. E. Albadri, M. A. B. Aissa, A. Modwi, and S. M. Saleh, "Synthesis of mesoporous Ru-ZnO g-C_3N_4 nanoparticles and

their photocatalytic activity for methylene blue degradation," *Water*, vol. 15, no. 3, p. 481, 2023.

[13] S. M. Saleh, A. E. Albadri, M. A. B. Aissa, and A. Modwi, "Fabrication of mesoporous V_2O_5@ g-C_3N_4 nanocomposite as photocatalyst for dye degradation," *Crystals*, vol. 12, p. 1766, 2022.

[14] W. Abdussalam-Mohammed, "Comparison of chemical and biological properties of metal nanoparticles (Au, Ag), with metal oxide nanoparticles (ZnO-NPs) and their applications," *Advanced Journal of Chemistry, Section A*, vol. 3, 2020.

[15] H. M. Fahmy, A. M. Mosleh, A. A. Elghany et al., "Coated silver nanoparticles: synthesis, cytotoxicity, and optical properties," *Royal Society of Chemistry Advances*, vol. 9, no. 35, pp. 20118–20136, 2019.

[16] K. P. Steckiewicz, P. Cieciórski, E. Barcińska et al., "Silver nanoparticles as chlorhexidine and metronidazole drug delivery platforms: their potential use in treating periodontitis," *International Journal of Nanomedicine*, vol. 17, pp. 495–517, 2022.

[17] J. M. Domingues, C. S. Miranda, N. C. Homem, H. P. Felgueiras, and J. C. Antunes, "Nanoparticle synthesis and their integration into polymer-based fibers for biomedical applications," *Biomedicines*, vol. 11, no. 7, p. 1862, 2023.

[18] S. N. Nandhini, N. Sisubalan, A. Vijayan et al., "Recent advances in green synthesized nanoparticles for bactericidal and wound healing applications," *Heliyon*, vol. 9, no. 2, Article ID e13128, 2023.

[19] P. K. Dikshit, J. Kumar, A. K. Das et al., "Green synthesis of metallic nanoparticles: applications and limitations," *Catalysts*, vol. 11, no. 8, p. 902, 2021.

[20] A. Singh, B. Madhavi, and M. N. Nithin Sagar, "An overview of green synthesis mediated metal nanoparticles preparation and its scale up opportunities," *Journal of Drug Delivery and Therapeutics*, vol. 11, no. 6, pp. 304–314, 2021.

[21] A. Zuhrotun, D. J. Oktaviani, and A. N. Hasanah, "Biosynthesis of gold and silver nanoparticles using phytochemical compounds," *Molecules*, vol. 28, no. 7, pp. 3240–3331, 2023.

[22] R. R. Patel, R. R. Patel, S. K. Singh, and M. Singh, "Green synthesis of silver nanoparticles: methods, biological applications, delivery and toxicity," *Materials Advances*, vol. 4, no. 8, pp. 1831–1849, 2023.

[23] C. Buzea, I. I. Pacheco, and K. Robbie, "Nanomaterials and nanoparticles: sources and toxicity," *Biointerphases*, vol. 2, no. 4, p. MR17, 2007.

[24] A. Malakar, S. R. Kanel, C. Ray, D. D. Snow, and M. N. Nadagouda, "Nanomaterials in the environment, human exposure pathway, and health effects: a review," *Science of the Total Environment*, vol. 759, Article ID 143470, 2021.

[25] B. A. Abbasi, J. Iqbal, J. A. Nasir et al., "Environmentally friendly green approach for the fabrication of silver oxide nanoparticles: characterization and diverse biomedical applications," *Microscopy Research and Technique*, vol. 83, no. 11, pp. 1308–1320, 2020.

[26] K. S. Siddiqi, A. Husen, and R. A. K. Rao, "A review on biosynthesis of silver nanoparticles and their biocidal properties," *Journal of Nanobiotechnology*, vol. 16, pp. 14–28, 2018.

[27] A. Rónavári, N. Igaz, D. I. Adamecz et al., "Green silver and gold nanoparticles: biological synthesis approaches and potentials for biomedical applications," *Molecules*, vol. 26, no. 4, p. 844, 2021.

[28] P. Tippayawat, N. Phromviyo, P. Boueroy, and A. Chompoosor, "Green synthesis of silver nanoparticles in aloe vera plant extract prepared by a hydrothermal method and their synergistic antibacterial activity," *PeerJ–the Journal of Life and Environmental Sciences*, vol. 4, Article ID e2589, 2016.

[29] H. M. Ibrahim, Q. Y. M. Abdullah, A. A. Humaid, A. A. M. Tabit, and S. M. A. A. Al-alawi, "Phytochemical screening and anti-microbial activities of aloe fleurentinorum lavranos & Newton," *Journal of Chemical, Biological and Physical Sciences*, vol. 12, pp. 335–348, 2022.

[30] O. M. Grace, "The Aloe names book," *Choice Reviews Online*, vol. 49, pp. 49–6878, 2012.

[31] R. R. Klopper and G. F. Smith, "Aloes of the world: when, where and who?" *Aloe*, vol. 50, pp. 44–52, 2013.

[32] R. Pandey and A. Mishra, "Antibacterial activities of crude extract of aloe barbadensis to clinically isolated bacterial pathogens," *Applied Biochemistry and Biotechnology*, vol. 160, no. 5, pp. 1356–1361, 2010.

[33] A. W. A. Al-Khulaidi, A. H. Al-Qadasi, and O. S. S. Al-Hawshabi, "Natural plant species inventory of the important plant areas in arabian peninsula: bani omar, taiz governorate, Republic of Yemen," *Electronic Journal of University of Aden for Basic and Applied Sciences*, vol. 1, no. 3, pp. 135–150, 2020.

[34] A. N. Al-Hakimi, T. M. Alresheedi, and R. A. Albarrak, "The effect of the Saudi haloxylon ammodendron shrub on silver nanoparticles: optimal biosynthesis, characterization, removability of mercury ions, antimicrobial and anticancer activities," *Inorganics*, vol. 11, no. 6, pp. 246–316, 2023.

[35] Y. M. S. Jamil, M. A. H. Awad, H. M. A. Al-Maydama, Y. El-Ghoul, and A. N. Al-Hakimi, "Synthesis and study of enhanced electrochemical properties of NiO nanoparticles deposited on TiO2 nanotubes," *Applied Organometallic Chemistry*, vol. 36, no. 9, pp. 1–15, 2022.

[36] T. Shuga, H. Elsayed, A. Mohamed, and M. Maaza, "ZnO nanoparticles prepared via a green synthesis approach: physical properties, photocatalytic and antibacterial activity," *Journal of Physics and Chemistry of Solids*, vol. 160, pp. 1–13, 2021.

[37] P. J. Burange, M. G. Tawar, R. A. Bairagi et al., "Synthesis of silver nanoparticles by using Aloe vera and Thuja orientalis leaves extract and their biological activity: a comprehensive review," *Bulletin of the National Research Centre*, vol. 45, no. 1, pp. 181–213, 2021.